Dynamic Effects of Ventral Hippocampal NRG3/ERBB4 Signaling on Nicotine Withdrawal-Induced Responses

Miranda L. Fisher Ph.D.[1], Emily R. Prantzalos B.S.[1], Bernadette O'Donovan Ph.D.[2], Tanner Anderson B.S.[3], Pabitra K. Sahoo Ph.D.[4], Jeffery L. Twiss M.D. Ph.D.[4], Pavel I. Ortinski Ph.D.[3], Jill R. Turner Ph.D.[1]

[1] Department of Pharmaceutical Sciences, University of Kentucky College of Pharmacy, Lexington, Kentucky, USA

[2] Department of Anesthesiology, Duke University School of Medicine, Durham, North Carolina, USA

[3] Department of Neuroscience, University of Kentucky College of Medicine, Lexington, Kentucky, USA

[4] Department of Biological Sciences, University of South Carolina College of Arts and Sciences, Columbia, South Carolina, USA

Correspondence should be addressed to:
Dr. Jill Turner, PhD
University of Kentucky
College of Pharmacy
789 S. Limestone Street
473 Lee T. Todd Jr. Building
Lexington, KY 40536-0596
P: 859-218-1025
E: Jill.Turner@uky.edu

Abstract

Tobacco smoking remains a leading cause of preventable death in the United States, with a less than 5% success rate for smokers attempting to quit. High relapse rates have been linked to several genetic factors, indicating that the mechanistic relationship between genes and drugs of abuse is a valuable avenue for the development of novel smoking cessation therapies. For example, various single nucleotide polymorphisms (SNPs) in the gene for neuregulin 3 (*NRG3*) and its cognate receptor, the receptor tyrosine-protein kinase erbB-4 (*ERBB4)*, have been linked to nicotine addiction. Our lab has previously shown that ERBB4 plays a role in anxiety-like behavior during nicotine withdrawal (WD); however, the neuronal mechanisms and circuit-specific effects of NRG3-ERBB4 signaling during nicotine and WD are unknown. The present study utilizes genetic, biochemical, and functional approaches to examine the anxiety-related behavioral and functional role of NRG3-ERBB4 signaling, specifically in the ventral hippocampus (VH). We report that 24hWD from nicotine is associated with altered synaptic expression of VH NRG3 and ERBB4, and genetic disruption of VH *ErbB4* leads to an elimination of anxiety-like behaviors induced during 24hWD. Moreover, we observed attenuation of GABAergic transmission as well as alterations in Ca^{2+}-dependent network activity in the ventral CA1 area of VH *ErbB4* knock-down mice during 24hWD. Our findings further highlight contributions of the NRG3-ERBB4 signaling pathway to anxiety-related behaviors seen during nicotine WD.

50 **Introduction**

51   Nicotine addiction impacts 1.2 billion people worldwide, with more people addicted to nicotine than any

52 other drug [1]. Abstinence from chronic nicotine use results in both cognitive and affective withdrawal (WD)

53 symptoms, which can be observed just a few hours after discontinuation of nicotine use [2] and are suggested

54 to be the predominant factors in driving relapse to cigarette smoking [3]. Supporting data link hippocampal

55 function with nicotine WD-induced phenotypes in both humans [4-8] and rodents [9-12]. However, mounting

56 evidence suggests that the hippocampus is not a homogenous structure, but instead, it can be divided into dorsal

57 and ventral regions, each mediating different behaviors [13]. Our lab has previously reported that these

58 subregional functional differences correspond with distinct WD phenotypes. We found that cAMP response

59 element-binding protein (CREB) activity, specifically in the ventral hippocampus (VH), mediates anxiety-like

60 behaviors in mice undergoing 24hWD, whereas dorsal hippocampal (DH) CREB activity mediates cognitive

61 effects [14]. Furthermore, to elucidate potential CREB target genes underlying these phenotypes, we evaluated

62 CREB binding genome-wide following chronic nicotine exposure and WD using chromatin immunoprecipitation

63 and whole-genome sequencing. These experiments showed that CREB is highly enriched at the promoter for

64 the Neuregulin-3 (*Nrg3*) gene following chronic nicotine and WD in the hippocampus [15].

65   NRG3 is a neuronal-enriched member of the epidermal growth factor-like (EGF-like) family of Neuregulins

66 1-6. NRG3's expression is limited to the CNS, where its EGF-like domain binds exclusively to receptor tyrosine-

67 protein kinase erbB-4 (ERBB4) receptors [16] enriched in neuronal post-synaptic densities (PSD) of inhibitory

68 interneurons [17-19]. In situ hybridization studies show that *Nrg3* and *ErbB4* have the highest expression in

69 cortical and hippocampal regions [16], where their interactions play pleiotropic roles in brain development and

70 plasticity. NRG3 was identified as a chemoattractive factor regulating GABAergic interneuron migration through

71 its interaction with ERBB4 in the developing brain [20]. NRG3-ERBB4's involvement in the assembly and

72 maturation of inhibitory circuitry is particularly noteworthy due to its association with a wide variety of

73 neurodevelopmental and neuropsychiatric disorders [21]. Less is known about this pathway's function in the

74 adult brain, but it is speculated to remain involved in activity-dependent synaptic formation and maintenance.

75 Addictive drugs are known to cause persistent restructuring of several different neuronal subtypes resulting in

76 long-term changes in synaptic plasticity. We have previously demonstrated that ERBB4 activation is necessary

3

77   for nicotine-induced plasticity in the orbitofrontal cortex, a region associated with impulse control [22].

78   Additionally, our previous investigations revealed that ERBB4 antagonism attenuates anxiety-like behavior

79   during chronic nicotine WD [15]. However, circuit-specific effects of NRG3-ERBB4 signaling on the affective

80   measures of prolonged nicotine exposure and WD have yet to be previously determined.

81   Genetic association studies from our lab and collaborators indicate a significant association of multiple

82   *NRG3* and *ERBB4* single nucleotide polymorphisms (SNPs) with smoking cessation outcomes [15,23]. While

83   there is persuasive evidence for the role of NRG3-ERBB4 signaling in nicotine dependence, the precise activity

84   of these signaling molecules and the neural adaptations they regulate during WD from nicotine is unknown.

85   Therefore, this study aims to systematically investigate the VH ERBB4 signaling during chronic nicotine and WD.

86   We found that selective deletion of VH *ErbB4* attenuates anxiety-like behavior during nicotine WD. This anxiolytic

87   effect was accompanied by reductions in inhibitory synaptic transmission and alterations in network activity of

88   ventral CA1 pyramidal neurons.

89

90   **Results**

91   *24hWD from nicotine induces Nrg3 transcription in the ventral hippocampus*

92   NRG3 and ERBB4 are highly enriched at excitatory synapses onto interneurons within the VH [33]. To

93   determine nicotine effects on NRG3 and ErbB4 expression in this structure, wild-type *ErbB4*-floxed mice were

94   treated with intermittent saline or nicotine (12 mg/kg/day) and were subjected to 24h or 1week of WD. Ventral

95   hippocampal tissues collected from treated mice were used for mRNA and protein analysis.

96   RTqPCR analysis of wild type *ErbB4*-floxed mice revealed that VH *Nrg3* mRNA levels are increased at

97   the 24hWD time point and return to baseline by 1week, compared to chronic nicotine treated mice, suggesting

98   alterations in *Nrg3* synthesis occur early during nicotine abstinence and return to baseline within 1week of WD

99   ($F_{(3,33)}=3.653$, p=0.0223; one-way ANOVA; NIC versus 24hWD: p=0.0117; NIC versus 1week WD: p=0.3933;

100 post hoc analyses) (Fig.1Ai). No differences were observed in *ErbB4* mRNA levels during saline, nicotine, or

101 either WD time point ($F_{(3,33)}=0.8802$, p=0.4614; one-way ANOVA) (Fig.1Aii). Western blot analyses of the

102 75kDa band detected using the anti-NRG3 antibody revealed an increase in synaptosomal NRG3 protein during

103 24hWD, compared to saline control mice ($F_{(2,22)}=4.923$, p=0.0171; one-way ANOVA; SAL versus 24hWD:

4

104   p=0.0128; post hoc analyses) (Fig.1Bi). Synaptosomal fractions immunoblotted with the affinity-purified anti-

105   ERBB4 antibody yielded major bands at 180, 120, and 80kDa [34]. The full-length 180kDa band (F(2,22)=6.974,

106   p=0.0045; one-way ANOVA; NIC vs. 24hWD: p=0.0036) and the 120kDa band (F(2,21)=7.566, p=0.0034; one-

107   way ANOVA; SAL versus 24hWD: p=0.0024) of ERBB4 were significantly increased during 24hWD, compared

108   to their chronic nicotine or saline-treated counterparts (Fig.1Bii,iii). A qualitatively similar effect observed at the

109   80kDa band was not significant (Fig.1Biv) (F(2,20)=1.855, p>0.05).

110

111   *Decreased ErbB4 within the VH attenuates 24hWD-induced transcription of Nrg3 mRNA*

112   To target ErbB4 signaling in the VH, we performed stereotaxic microinjections of AAV-CRE, or AAV-RFP

113   control virus, into the VH of the *ErbB4*-floxed mouse line. RFP viral expression in the VH is shown in the

114   *Supplementary Information* to demonstrate appropriate targeting of the viral construct (Fig.S1A). These animals

115   were treated chronically with saline or nicotine and underwent 24h of nicotine withdrawal before behavioral

116   testing (Fig.2A). RTqPCR analysis of VH tissue demonstrated CRE recombinase expression was significantly

117   higher in CRE-injected mice, compared to RFP-controls (t(70)=6.059 p<0.0001; unpaired t-test) (Fig.S1B). This

118   increase in CRE recombinase expression resulted in a significant interaction and main effect of genotype and

119   reduced *ErbB4* mRNA levels to ~60% of that of RFP SAL mice (main effect of genotype F(1,66)=121.0,

120   p<0.0001; two-way ANOVA; RFP SAL versus CRE SAL: p<0.0001, CRE NIC: p<0.0001, CRE 24hWD:

121   p<0.0001, Post-hoc analyses) (Fig.2B). Furthermore, *Nrg3* mRNA expression analyses showed an interaction

122   and main effect of genotype, with increased *Nrg3* expression in RFP 24hWD mice compared to their NIC treated

123   counterparts (main effect of genotype F(1,66)=12.37, p<0.005; interaction F(2,66)=10.90, p<0.0001; two-way

124   ANOVA; RFP SAL versus RFP 24hWD: p=0.0018, post hoc analyses) (Fig.2C). This increase in *Nrg3* mRNA

125   was not observed in CRE-injected mice (no treatment effect, F(2,31=1.982, p>0.05; one-way ANOVA) (Fig.2C).

126

127   *VH ErbB4 knock-down blocks anxiogenic behavior measured in the NIH test*

128   We next performed behavioral analyses to evaluate the influences of VH *ErbB4* KD on anxiety-like

129   behaviors. The NIH test is a well-validated measure for VH-dependent anxiety-related behaviors that is sensitive

130   to acute anxiolytics and chronic antidepressants [35]. No genotype effects were observed during training in

5

131   latency to consume prior to treating mice with saline or nicotine (t(5)=2.162, p>0.05; paired t-test) (Fig.2Di) or

132   amount consumed (t(70)=0.02770, p>0.05; unpaired t-test) (Fig.2Dii). Mice then underwent two weeks of chronic

133   treatment of saline or nicotine via osmotic minipumps. To confirm there were no appetitive effects of chronic

134   nicotine treatment, mice were presented with peanut butter chips (PB) in their home cage, and latency was

135   measured (Home Test Day). No significant difference between groups was observed (F(5,66)=1.072, p=0.3940;

136   one way ANOVA) (Fig.2Diii). After Home Test Day, osmotic minipump removal and sham surgeries were

137   performed to induce WD. After 24hWD, mice were placed in a novel environment (Novel Test Day) and again

138   latency to feed was measured, displaying an interaction and main effect of treatment, and day (main effect of

139   day, F(1, 131)=147.6, p<0.0001; main effect of treatment F(5, 131)=7.281, p<0.0001; interaction F(5,

140   131)=7.458, p<0.0001) (Fig.2Diii). RFP mice undergoing 24hWD displayed a significant increase in latency to

141   feed on novel test day compared to controls (RFP SAL versus RFP 24hWD: p=0.0302; post hoc analyses), while

142   CRE-injected animals showed a significant reduction in latency to feed across all treatment groups, compared

143   to RFP SAL control mice (RFP SAL versus CRE SAL: p=0.0009; CRE NIC: p=0.0006; CRE 24hWD: p=0.0005;

144   post-hoc analyses) (Fig.2Diii). No sex differences were observed.

145   After NIH testing was conducted, mice were placed in their home cages for a 1h recovery period before

146   the Open Field exploration test was run that afternoon. Representative traces show activity in the Open Field

147   arena of RFP- and CRE-injected 24hWD groups (Fig.2Ei). Results from this test indicated a significant treatment

148   effect (F(1,66)=5.148, p<0.05; two-way ANOVA) (Fig.2Eii). Control mice undergoing 24hWD (RFP 24hWD)

149   displayed a significant decrease in time spent in the center arena, compared to SAL controls (p=0.0290),

150   indicative of an anxiogenic response to a novel environment during WD (Fig.2Eii). Interestingly, in CRE-injected

151   VH *ErbB4* KD mice, this treatment effect was undetectable, with no significant differences between SAL and

152   24hWD groups (RFP SAL versus RFP 24hWD: p=.9994; post hoc analyses) (Fig.2Eii). No locomotor deficits

153   were observed between genotypes or treatments (no interaction F(2,64)=0.4727, p>0.05; two-way ANOVA)

154   (Fig.2Eiii). Collectively, findings from both behavioral tests suggest that disruption of NRG3-ERBB4 activity in

155   the VH attenuates prominent anxiogenic effects induced during 24hWD.

156

157   *ErbB4 mRNA expression predominates in the CA1 area of the ventral hippocampus*

158   The hippocampus has a very well-defined architecture consisting of populations of excitatory principal

159   neurons assembled into distinct regions: the dentate gyrus (DG), and areas CA3-CA1. These areas form what

160   is known as the trisynaptic circuit, an information flow beginning with cortical inputs from the entorhinal cortex

161   (EC), which carry higher-order spatial and contextual information, synapsing onto DG granule cells via perforant

162   path fibers. Mossy fibers from DG granule cells project to pyramidal neurons of the CA3 which form schaffer

163   collaterals innervating CA1 pyramidal cells. Axons of CA1 pyramidal neurons in turn target both intra-

164   hippocampal and extra-hippocampal territories [36]. It is well-accepted that the different circuit components along

165   this pathway (DG, CA3, CA1) contribute to unique aspects of memory and emotional processing [37]. Therefore,

166   circuit-specific expression and functional patterns of NRG3 and ERBB4 may provide insights into how this

167   signaling pathway modulates circuit-level events underlying affective behaviors during nicotine WD. To this end,

168   we used smFISH to visualize and quantify individual *Nrg3* and *ErbB4* mRNA puncta signals within the VH

169   subregions. In Figure 3Ai, a representative 10x image of the VH illustrates patterns of peri-nuclear expression

170   (Fig.3Ai). Images of the subregions DG, CA3, and CA1 of the VH, highlighted in yellow in the right (Fig.3Aii),

171   were taken with a 63x oil objective to observe expression patterns of *Nrg3* (Fig.3B) and *ErbB4* mRNAs (Fig.3D).

172   Quantitative analysis using ImageJ showed consistent expression of *Nrg3* mRNA within the DG, CA3, and CA1

173   areas of the VH, with no significant differences between regions ($F_{(2,6)}=1.659$, $p>0.05$; one way ANOVA)

174   (Fig.3C). Conversely, quantification of *ErbB4* mRNA showed a significant difference in signal between the CA1

175   and DG ($F_{(2,6)}=8.977$, $P<0.05$; one way ANOVA), with the highest expression of *ErbB4* mRNA present in the

176   CA1 area of the VH (DG versus CA1, $p=0.0138$) (Fig.3E).

177

178   *Ventral hippocampal ErbB4 knock-down reduces spontaneous IPSC and miniature IPSC frequencies in the*

179   *ventral CA1*

180   Given its central output role and high NRG3/ERBB4 expression, we next investigated the functional

181   impact of ERBB4 on ventral CA1 neuronal activity during 24hWD. *ErbB4*-floxed animals underwent stereotaxic

182   microinjections of either AAV-RFP+ GCaMP6f (control) or AAV-CRE+ GCaMP6f (*ErbB4* KD) in the VH, allowing

183   for collection of electrophysiological and Ca^{2+} imaging recordings of CA1 pyramidal neurons from the same

184   subject during the 24hWD condition. Using whole-cell patch-clamp electrophysiology, we first evaluated the

7

185   effect of VH *ErbB4* KD on spontaneous excitatory and inhibitory postsynaptic currents (sEPSCs and sIPSCs)

186   (Figure 4Ai/Bi), as well as action-potential independent miniature excitatory and inhibitory postsynaptic currents

187   (mEPSCs and mIPSCs) in CA1 pyramidal cells. VH *ErbB4* KD significantly reduced sIPSC frequency in CA1

188   pyramidal neurons ($t(17)=3.228$ $p<0.01$; unpaired t-test) (Fig.4Aii), with no significant changes in sIPSC

189   amplitude ($t(17)=0.4036$ $p>0.05$; unpaired t-test) (Fig.4Aiii). The mIPSC data also showed reduced frequency of

190   synaptic events ($t(11)=2.612$ $p<0.05$; unpaired t-test) (Fig.4Aiv); however, we also observed an increase in

191   mIPSC amplitude ($t(11)=3.994$ $p<0.01$; unpaired t-test) (Fig.4Av). No differences in either sEPSC frequency

192   ($t(16)=0.6112$ $p>0.05$; unpaired t-test) (Fig.4Bii) or amplitude ($t(17)=1.195$ $p>0.05$; unpaired t-test) (Fig.4Biii) or

193   mEPSC frequency ($t(14)=0.9388$ $p>0.05$; unpaired t-test) (Fig.4Biv) or amplitude ($t(14)=0.6612$ $p>0.05$; unpaired

194   t-test) (Fig.4Bv) were observed in the KD mice undergoing 24hWD compared to controls. These findings show

195   that in mice undergoing 24hWD, *ErbB4* deletion primarily impacts inhibitory synaptic transmission onto CA1

196   pyramidal neurons in the VH.

197

198   *Ventral hippocampal ErbB4 knock-down impacts CA1 network activity during 24hWD*

199   After observing alterations in inhibitory input onto individual CA1 pyramidal cells, we next queried whether

200   these effects impacted overall network activity between genotypes using wide-field Ca^{2+} imaging. We monitored

201   fluorescence of the hSYN-driven Ca^{2+} sensor, GCaMP6f [38], in the ventral CA1 of RFP and VH *ErbB4* KD mice

202   undergoing 24hWD (regions of interest, ROIs, Fig.4C). Given the importance of inhibitory signaling on patterning

203   of pyramidal cell output in the hippocampus [39], we evaluated the effect of ErbB4 KD on two measures of

204   network segregation: community structure and network clustering. Quantification of spontaneous (baseline) and

205   evoked Ca^{2+} transients showed no difference in the number of communities between RFP and CRE-injected

206   mice across stimulation intensities (no interaction, $F(3,39)=0.04595$, $p>0.05$; RM two-way ANOVA) (Fig.4D).

207   Furthermore, we found no differences in the network clustering coefficient across stimulation intensities in wild

208   type RPF 24hWD mice ($F(2.364, 14.18)=0.04814$, $p>0.05$, RM one way ANOVA) (Fig.4E). In contrast, CRE

209   24hWD mice displayed a significant reduction in network clustering ($F(1.996, 13.97)=5.124$, $p<0.05$; RM one

210   way ANOVA) at the minimum (BASELINE versus MIN. STIM: $p=0.0419$; post hoc analyses) and 2x (BASELINE

211   versus 2x STIM: $p=0.0497$; post hoc analyses) stimulation intensities compared to baseline (Fig.4E). These data

212 indicate that ErbB4 KD increased sensitivity of the hippocampal network to electrical stimuli at 24hWD from

213 chronic nicotine.

214

215 **Discussion**

216   Cumulative evidence indicates that while the positive reinforcing effects of nicotine play a crucial role in

217 the development of nicotine dependence, negative reinforcers, such as WD symptoms, drive the maintenance

218 of nicotine dependence similar to other stimulants [40]. For example, the ability of nicotine to alleviate the

219 negative affective states occurring during WD can directly lead to relapse after periods of abstinence [41-43].

220 Our previous studies demonstrated that chronic nicotine WD elicits anxiogenic effects [14,15,26] that are

221 precluded by systemic pharmacological blockade of ERBB4 receptors [15]. In this study, we used genetic,

222 biochemical, and functional approaches to investigate NRG3-ERBB4 neural correlates within the brain anxiety

223 circuitry during chronic nicotine exposure and WD. At the cellular level, both *Nrg3* and *ErbB4* mRNAs increased

224 in the VH at 24hWD. Moreover, attenuation of anxiety-like phenotypes in VH *ErbB4* KD mice was accompanied

225 by alterations in inhibitory transmission and overall network activity in the CA1 area, a subregion of the VH

226 enriched in *Nrg3* and *ErbB4* mRNAs, during 24hWD from chronic nicotine. Thus, our findings determined that

227 NRG3 and its cognate receptor ERBB4 are necessary for the manifestation of anxiety-like behavior during

228 nicotine WD, a hallmark symptom seen in mice [44,45] and humans [4,46,47]. Therefore, in agreement with our

229 previous studies [15,22], our data provide compelling evidence that the NRG3-ERBB4 signaling pathway

230 represents a causal and druggable mechanism in the expression of nicotine WD phenotypes.

231

232 *Synaptic expression of ventral hippocampal* NRG3 *and* ERBB4 *are induced during 24hWD*

233   Active gene transcription is necessary for addiction processes. However, divergent gene networks may

234 underlie various addiction phenotypes. As mentioned previously, CREB is a well-established transcription factor

235 in the field of addiction [48-50]. It is crucial for stimulus-transcription coupling, in which events occurring at the

236 cell surface leads to alterations in gene expression and ultimately changing neuronal protein expression. Our lab

237 has previously demonstrated that increases in total and phosphorylated levels of CREB are present during

238 chronic nicotine and 24hWD in the hippocampus, leading to increased transcription of the CREB target gene,

9

239   *Nrg3* [15]. In the present study, we detected increased *Nrg3* transcripts specifically at the 24hWD time point

240   within the VH, with 1 week post WD mRNA levels of *Nrg3* returning to baseline. Interestingly, this increase in

241   *Nrg3* transcription falls within the timeline of observable nicotine WD signs in rodents—being the most severe

242   24-48 h post- WD and tapering off after this timepoint [51]. Similarly, studies in smokers show that WD symptoms

243   set in between 4-24 hours after an individual smokes their last cigarette, with the symptoms peaking at around

244   day 3 [52]. Moreover, smokers exhibit functional and morphological changes in the hippocampus during

245   abstinence [53,54].

246   24hWD-induced molecular changes were also seen at the protein level, with increased NRG3 and

247   ERBB4 protein levels in synaptic fractions. Previous studies have demonstrated synaptic enrichment of these

248   proteins, where they participate in the formation and maintenance of synapses [21,33,55,56]. Western blotting

249   of VH synaptosomal fractions showed the presence of the full-length NRG3 (75kDa) [57] and full-length ERBB4

250   (180kDa) along with cleavage products (120kDa and 80kDa bands) [34,58], all of which were upregulated at

251   24hWD (Fig.1B). NRG binding is implicated in the shedding of a 120kDa ectodomain fragment via cleavage by

252   the metalloprotease TNF-α-converting enzyme (TACE) [34]. Subsequent cleavage by presenilin/gamma

253   secretases releases an 80kDa intracellular domain with an active tyrosine kinase domain and can translocate to

254   the nucleus and promote nuclear transcription of various transcription factors [59,60]. ERBB4 appears to be the

255   only erbB that harbors a nuclear localization signaling in its intracellular domain [61]. Our data suggest that

256   24hWD not only induces translation of the full-length precursor ERBB4 further but provokes proteolytic cleavage

257   as well (Fig.1Bii-iv). Further experimentation is necessary to determine the precise role of nuclear ERBB4

258   signaling during WD.

259

260   *Ventral hippocampal* ERBB4 *signaling mediates WD-induced anxiety-like behaviors*

261   We found that increased expression of NRG3-ERBB4 signaling in the VH corresponds to anxiety-like

262   behaviors, with genetic disruption of this pathway eliminating these phenotypes induced during 24hWD. The NIH

263   test and the Open Field exploratory tests model ascertains anxiety-like behaviors in rodents by integrating an

264   approach-avoidance conflict paradigm [62]. Our behavioral data is in accordance with our previous studies

265   [15,24-26,63], revealing anxiety-like responses increase during 24hWD. These findings suggest that abstinence

10

266 from nicotine is an additional stressor that promotes anxiogenic behaviors when placed in an unfamiliar

267 environment, a phenotype detected in both the NIH and OF tests.

268   The OF test revealed that VH *ErbB4* deletion has an anxiolytic effect on 24hWD-dependent exploratory

269 behavior in an unfamiliar environment. Yet, the NIH test demonstrated a significant baseline difference in the

270 latency to feed in VH *ErbB4* KD mice across all treatments on Novel Test Day. These findings suggest that

271 *ErbB4* deletion produces a floor effect in this paradigm, where anxiety-like responses are at such a low threshold

272 that no treatment effects are detectable. Baseline levels of hyponeophagia in mice can be influenced by genetic

273 background, isolated housing, and specific genetic mutations that affect anxiety-related behaviors [64,65].

274 Approach-avoidant paradigms are common exploration-based tests for anxiety-like behaviors, based on the

275 premise that novel environmental stimuli may be perceived as threatening and thereby inhibit the innate tendency

276 to explore. The NIH and OF assays both rely on response to novel stimuli, therefore our data may alternatively

277 indicate alterations in novelty-seeking phenotypes rather than the described impact on avoidance. Nonetheless,

278 altered novelty-seeking and harm avoidance are both putatively linked to increased risk for drug abuse, as well

279 as anxiety and related disorders [66-69].

280   Current literature examining pharmacological and genetic manipulations of NRG3 and ERBB4 signaling

281 in the brain result in a similar display of abnormal affective behaviors in mice, strengthening our evidence that

282 *ErbB4* KD impacts anxiety-related behavior. In adult mice, neonatal overexpression of NRG3 results in increased

283 impulsive action, heightened anxiety, and reduced social function [70]. *ErbB4* KD models report that deletion of

284 *ErbB4* from interneurons in the cortex and hippocampus results in decreased anxiety [71-73]. Conversely, it

285 seems this signaling pathway may mediate opposing behaviors in other brain regions. For example, *ErbB4*

286 deletion from serotonergic neurons in the dorsal raphe nucleus engenders anxiogenic behaviors, which is

287 reversed by the inactivation of this subset of neurons [74]. In the amygdala, deletion of *ErbB4* from somatostatin

288 (SOM+)-expressing interneurons also increases anxiety [75], whereas administration of NRG1 alleviates anxiety

289 and enhances GABAergic transmission [76]. Additionally, blocking NRG1-ERBB4 signaling in the bed nucleus

290 of the stria terminalis (BNST) region had anxiogenic effects on behavior as well [77]. These data provide

291 evidence of brain region and circuitry-specific modulation of NRG-ERBB4 signaling on select phenotypes.

292 Recent studies have shown that ventral CA1 cell projections, the primary output of the hippocampal formation,

11

293 mediate anxiety-like behavior via reciprocal communication with the medial prefrontal cortex (mPFC) [78-82],

294 hypothalamus [83], and amygdala [84,85]. Therefore, these findings support the hypothesis that *ErbB4* deletion

295 could attenuate the effects 24hWD has on VH specific function and its associated circuitry.

296

297 *Ventral hippocampal ErbB4 knock-down mice have decreased sIPSC and mIPSC frequencies and dysregulated*

298 *network clustering in the CA1 area during 24hWD*

299 The impact of VH *ErbB4* deletion on pyramidal cell dynamics during 24hWD is unknown. smFISH

300 experiments demonstrated the highest expression of *ErbB4* mRNA in the CA1 area. In addition to pyramidal

301 cells, there are over 20 types of GABAergic inhibitory interneurons in the CA1 subregion alone [86]. ERBB4

302 protein is particularly enriched in postsynaptic terminals of parvalbumin (PV+) and cholecystokinin (CCK+)-

303 expressing GABAergic interneurons within the hippocampus [87-89]. Within the hippocampus and the cortex,

304 NRG3 expression is restricted to excitatory presynaptic pyramidal cell terminals contacting interneurons,

305 promoting formation and maturation of excitatory synapses onto ERBB4+ interneurons [33,55,90]. ERBB4

306 regulates GABAergic neurotransmission, synaptic plasticity, and neuronal activity in cortical areas [88,91,92]. In

307 our study, GABAergic synaptic transmission was weakened in VH *ErbB4* KD mice during 24hWD, characterized

308 by a significant reduction in the frequency of sIPSCs and mIPSCs recorded from pyramidal neurons. A similar

309 IPSC frequency decrease has been previously reported after *ErbB4* deletion in fast-spiking interneurons [71].

310 Changes in synaptic current frequency, particularly at the level of action-potential independent mIPSCs, are

311 traditionally attributed to pre-synaptic mechanisms, suggesting deficits at the level of GABA releasing

312 interneurons. However, while we see no significant changes in sIPSC amplitude, a measure reflecting post-

313 synaptic GABA$_A$ receptor activation, we do find an increase in the amplitude of mIPSCs, as shown after *ErbB4*

314 deletion in the amygdala [93]. It is possible that post-synaptic receptor up-regulation compensates for reduced

315 GABA release after *ErbB4* KD in the VH. Given that mIPSC data isolates receptor responses at individual

316 synaptic boutons, differences in the effect of *ErbB4* KD on sIPSC and mIPSC amplitude may reflect additional

317 adaptations at the level of synaptic arborization following nicotine withdrawal.

318 Furthermore, the attenuation of mIPSC frequency was accompanied by altered network clustering,

319 suggesting a role for ERBB4 receptors on pyramidal cell ensembles through GABAergic transmission. For

320 example, deletion of the *ErbB4* gene reduces GABAergic transmission, increases the firing of pyramidal neurons,

321 and enhances long-term potentiation (LTP) in brain slices [91,94-96]. Additionally, recent evidence showed that

322 NRG3 strengthens excitatory synaptogenesis onto ERBB4-expressed GABAergic neurons and its functionality

323 in the hippocampus [33]. In the present study, we have not assessed whether ERBB4-induced GABAergic

324 neurotransmission during nicotine WD is NRG3-dependent. Nevertheless, our current and previous findings

325 indicating that nicotine exposure and WD increase gene and protein expression of NRG3, but not NRG1, are

326 consistent with this hypothesis [15].

327 The electrophysiology and Ca^{2+} imaging experiments were designed to evaluate the effect of VH ErbB4

328 KD on synaptic transmission and overall network excitability during 24h WD. Previous data from our lab has

329 examined the impacts of both nicotine and 24hWD on VH activity [26]. Using voltage-sensitive dye imaging, CA1

330 responsivity to schaffer collateral stimulation is increased following *in vivo* chronic nicotine treatment and returns

331 to saline levels after 24h of nicotine cessation; however, GABAergic tone remained disrupted following nicotine

332 withdrawal [26]. Therefore, in this study we focused on cell-selective molecular mechanisms potentially

333 contributing to the disinhibition observed during withdrawal. These data indicate that ERBB4 disruption

334 decreases inhibitory neurotransmission, likely resulting in reduced disinhibition of the CA1. This is in line with

335 the proposed compartmentalization of ERBB4-NRG3 signaling to hippocampal interneurons.

336

337 *Conclusion*

338 Our findings demonstrate contributions of VH specific ErbB4 signaling in anxiety-related behaviors seen

339 during nicotine WD. Mechanistically, NRG3-ERBB4 signaling disruption in the VH attenuates nicotine-induced

340 WD anxiogenic behaviors by altering GABAergic modulation of CA1 pyramidal cell activity. These findings

341 suggest that hindering NRG3 activation of ERBB4 at GABAergic synapses curtails inhibitory inputs and

342 regulation of excitatory pyramidal cell activity, and subsequent net output to other brain areas within the anxiety

343 circuitry. Our findings link neuronal mechanisms and circuit-specific effects of NRG3-ERBB4 signaling during

344 nicotine and WD to anxiety-like behaviors, suggesting that targeting NRG3-ERBB4 pathway may advance the

345 development of personalized therapies to smoking cessation.

346

Methods and Materials

Murine subjects

Male and female *ErbB4*-floxed mice (strain B6;129-*ErbB4*tm1Fej/Mmucd, stock number 010439-UCD) were cryo-recovered by the Mutant Mouse Resource and Research Centers (MMRRC), University of California, Davis. Live animals bred in house were 6-8 weeks of age at the beginning of experimentation. Mice were maintained on a 12 h light-dark cycle (lights on at 7:00 AM), with ad libitum food and water. All behavioral procedures were conducted during the hours of 9:00 AM – 5:00 PM. Protocols regarding the proposed work for these studies is approved by the University of Kentucky Institutional Care and Use Committee (IACUC) and the Institutional Biosafety Committee (IBC).

Stereotaxic surgery and ventral hippocampal microinjections

Surgery was performed on adult mice (6-8 weeks old). After induction of anesthesia with isoflurane (4%), mice were secured in a stereotaxic frame (Stoelting, Wood Dale, IL.). Mice were maintained under isoflurane anesthesia (1-2%) throughout the surgical procedure via a nose cone. Holes were drilled bilaterally into the skull at the injection sites. Ventral intrahippocampal stereotaxic coordinates were measured from the skull surface as follows: AP -2.9, ML ±3.0, DV -3.8. A 33-gauge needle attached to a 5 μl Hamilton syringe was mounted to the stereotaxic frame and, under control of a KDS310 Nano Pump (KD Scientific, Holliston, MA), was used to inject 0.5 μl of 1 x 10^9 gc/μl AAV at each site. Injections occurred at a rate of 0.1 μl/min, after which the needle was left in place for an additional 4 min. After injections were completed, the skin was sutured, and animals were given an intraperitoneal injection of 5 mg/kg meloxicam (Metacam, Boehringer, St. Joseph, MO) and allowed to recover for up to 1 h on a heating pad before being returned to their home cage. Mice remained in their home cage for an additional 4 weeks until the beginning of novelty-induced hypophagia (NIH) training. Reverse transcriptase coupled quantitative PCR (RTqPCR) analyses of *ErbB4* knock-down (KD) was assessed following all experiments and mice with less than a 20% KD of *ErbB4* in the VH were excluded from experiments.

Drugs and administration

14

373   (-)-Nicotine tartrate (MP Biomedicals, Solon, OH) was dissolved in 0.9% saline. Nicotine was

374 administered subcutaneously via osmotic minipumps (Alzet model 2002, Cupertino, CA) at a dose of 12 mg/kg/d

375 for 14 days, calculated based on the daily pump rate of the pulsatile delivery system (see "pulsatile delivery"

376 below). This dose, reported as freebase weight and based on previous work [15,24-26], corresponds to plasma

377 levels of ~0.2 µm [27], a concentration within the range observed in human smokers consuming an average of

378 12 cigarettes a day (plasma levels between 0.04 and 0.21 µm) [27].

379

380 *Osmotic minipumps surgeries*

381   <u>Pulsatile delivery.</u> A pulsatile nicotine delivery system was achieved by attaching osmotic minipumps to

382 polyethylene (PE60) tubing, similar to that described in Brynildsen and colleagues [28]. The PE60 tubing was

383 prepared using a coiling technique, which consisted of coiling the tubing around a cylinder with a similar

384 circumference to the minipump and dipping the thermoformable tubing in hot water, followed by immersion in

385 ice-cold water. This shaped the tubing into a coil for easy subcutaneous implantation. Once formed, the PE60

386 tubing was filled with alternating 0.5 µl volumes of nicotine tartrate (or saline for controls) and mineral oil. The

387 model 2002 osmotic minipumps used for experimentation have a delivery rate of 0.5 µl/hr, therefore we

388 developed a 1 hr "on", 1 hr "off" pulsatile nicotine delivery system. The attached PE60 tubing was filled to a

389 volume that ensured a time course of 14-day intermittent treatment.

390   <u>Minipump treatment groups.</u> In all experiments, animals were implanted with osmotic minipumps to

391 deliver pulsatile administration of either nicotine (12 mg/kg/day) or saline. Following 2 weeks of chronic

392 administration, mice were anesthetized with an isoflurane/oxygen vapor mixture (1–3%), an incision was made

393 above the pump at shoulder level, and the pump was either removed (to initiate a spontaneous WD from either

394 nicotine or saline) or left in place (to serve as sham surgical controls in the nicotine and saline groups). The

395 incision was then closed with 7 mm stainless steel wound clips. Animals were allocated to the different

396 experimental groups based on sex, pre-operative weight average, and behavioral baseline measures.

397

398 *Adeno-associated virus production*

15

399   The University of Pennsylvania Vector Core generated neuron-selective AAV serotype 9 for expressing:

400   Cre recombinase (AAV-CRE: AAV9.CMV.PI.Cre.rBG, titer 1.644 × 10^{13} genome copies (gc)/ml), red fluorescent

401   protein (AAV-RFP: AAV9.CMV.TurboRFP.WPRE.rBG, titer 32.87 × 10^{13} gc/ml), and GCaMP6f Ca^{2+} indicator

402   (AAV-9-PV2822: AAV9.Syn.GCaMP6f.WPRE.SV40). Purification of the vectors was performed using CsCl

403   sedimentation, and vector gc quantification was performed by the UPenn Vector core using qPCR. AAVs were

404   diluted in sterile PBS for microinjections directly into the VH. The University of Kentucky animal facility is

405   equipped to handle appropriate care of animals infected with AAV and all procedures are approved by IACUC.

406   All procedures utilizing AAV are also approved by our Institutional Biosafety Committee.

407

408   *Novelty-induced hypophagia (NIH) test*

409   The NIH test was performed as previously described [25]. Briefly, NIH training and testing consisted of

410   exposing mice to a highly palatable food (Reese's peanut butter chips (Nestle, Glendale, CA (ingredients:

411   partially defatted peanuts, sugar partially hydrogenated vegetable oil, corn syrup solids, dextrose, reduced

412   minerals whey, salt vanillin, artificial flavor, soy lecithin)) and latency to consume was measured. One week

413   before NIH training and for the duration of the experiment, mice were housed in groups of two. Training consisted

414   of daily sessions in which mice were exposed to Reese's peanut butter chips in a clear plastic dish. Plastic

415   dividers (dividing the standard mouse cage lengthwise) were placed inside each cage to separate the mice

416   during the training and home cage testing periods. Mice were acclimated to the barriers for 1 h before placement

417   of food. Food was placed in the cage for 15 min, and latency to consume was measured. By the 10th day, a

418   baseline latency to approach and consume the food was reached such that there was <20% variability between

419   mice. After the last training session, the amount consumed was recorded as grams of peanut butter chips to

420   ensure there were no appetitive treatment effects. Following training, mice were implanted with 14-day osmotic

421   minipumps filled with pulsatile nicotine (12 mg/kg/day) or 0.9% pulsatile saline. Testing in the home cage (Home

422   Test Day) and novel environment (Novel Test Day) occurred on the last 2 days of minipump viability. On Home

423   Test Day, following testing, minipumps were surgically removed for the WD groups, and sham surgeries were

424   performed on the chronic nicotine group as well as saline animals. Twenty-four hours later, on the Novel Test

425   Day, mice were removed from the home cage and placed in an empty standard cage with no bedding that had

16

426 been wiped with a cleanser (Pine-Sol, 1:10 dilution) to emit a novel odor and placed in a white box with bright

427 light illumination (2150 lux). Latency to consume the palatable food was recorded on both days.

428

429 *Open Field exploratory test (OF)*

430 The Open Field exploratory test is an anxiety-related behavioral model, which also allows simultaneous

431 assay of overall locomotor activity levels in mice. All mice were tested 24 h after nicotine minipumps were

432 removed from the 24h WD groups and sham surgeries were performed for the nicotine and saline groups. Test

433 chambers were wiped with 70% ethanol in between tests to remove any scent cues left by the previous mouse.

434 The ethanol was allowed to dry completely before each testing, and every testing session lasted for 10 min. For

435 the analysis, Top Scan (Clever Sys Inc., Reston, Virginia) software was utilized to track and evaluate mouse

436 movement. Prior to tracking analyses for each mouse, a background profile was generated, and the testing

437 chamber was calibrated in arena design mode according to the manufacturer's instructions. Software output for

438 each individual test includes total distance moved (in mm) and the time spent in the center (in %). These data

439 were then normalized to the AAV-RFP saline control group. On both behavioral paradigms, the data were

440 analyzed by an investigator blinded to the experimental groups.

441

442 *Reverse transcriptase coupled quantitative polymerase chain reaction (RTqPCR)*

443 RTqPCR was performed as previously described [29] on VH or DH samples across all treatment groups.

444 Briefly, RNA was isolated using the RNeasy Mini kit (Qiagen, Hilden, Germany), and 500 ng of RNA was reverse

445 transcribed into cDNA using Oligo dT primer (Promega, Madison, WI) and Superscript II reverse transcriptase

446 (Invitrogen, Waltham, MA). qPCR reactions were assembled using Thermo Scientific Maxima SYBR Green

447 master mix along with 100 nM primers (Eurofins Scientific, Luxembourg). The mRNA levels were determined

448 using the $2^{-\Delta\Delta CT}$ method [30], and target genes were normalized to the housekeeping gene Hypoxanthine

449 Phosphoribosyltransferase (HPRT). All gene expression values were normalized to their respective AAV-RFP

450 saline-treated controls. Primer sequences are shown in Table S1.

451

452 *Synaptosomal preparation*

453   To obtain synaptosomes, frozen VH tissue was weighed and gently homogenized with a glass dounce

454   tissue grinder in 10 vol (1:10, wt/vol) of Syn-PER synaptic protein extraction reagent (Thermo Fisher Scientific,

455   Rockford, IL) supplemented with a protease and phosphatase inhibitor cocktail. Following manufacturer's

456   instructions, the homogenate was centrifuged at 1200 xg for 10 min at 4°C, and then the supernatant was

457   centrifuged for a further 20 min at 1500 xg at 4°C. The supernatant (cytosolic fraction) was removed, and the

458   synaptosome pellets were resuspended in Syn-PER reagent. The protein concentrations of synaptosomal and

459   cytosolic fractions were determined by the BCA method (Thermo Fisher Scientific).

460

461   *Western blotting*

462   Protein analysis was performed as described previously on VH samples of all treatment groups. Briefly,

463   20 μg of protein was resolved in AnykD™ precast polyacrylamide gel (Bio-Rad Laboratories Inc., Hercules, CA)

464   and transferred to nitrocellulose membranes. Membranes were incubated with LI-COR blocking buffer (LI-COR,

465   Lincoln, NE) for 1 h at room temperature before reacting overnight at 4°C with primary antibodies: Neuregulin-3

466   (NRG3) (1:500, sc-67002, N-terminal extracellular domain, Santa Cruz Biotechnology, Santa Cruz, CA), ERBB4

467   (1:500, sc-283, Santa Cruz Biotechnology), and Beta-tubulin (1:2000, 2128L, Cell Signaling Technology,

468   Danvers, MA). After washing in phosphate-buffered saline-Tween-20 (PBST), the blots were incubated in

469   fluorescent secondary antibodies IRDye 800CW Goat anti-Mouse (1:20000, LI-COR) and IRDye 680LT Goat

470   anti-Rabbit (1:20000, LI-COR) diluted in LI-COR blocking buffer for 1 h at room temperature. Membranes were

471   then washed, and immunolabeling detection and densitometry measurements were performed using the LICOR

472   Odyssey System (LI-COR). Ratios of the proteins of interest (NRG3 and ERBB4) to the housekeeping protein

473   (β-tubulin) densities were calculated for each sample and normalized to AAV-RFP saline-treated controls. The

474   same Beta-tubulin control bands were used to calculate ErbB4 protein content on blots containing all three

475   densities of ErbB4 resulting from a single probe.

476

477   *Stellaris single-molecule fluorescent in situ hybridizations (smFISH)*

478   Forty-eight antisense 'Stellaris probes' oligonucleotide probes for mouse *Nrg3* and *ErbB4* were designed

479   using Biosearch custom design algorithms and synthesized with a 5' Quasar 570 and 670 labels, respectively.

18

One brain hemisphere from each mouse was collected and fixed overnight (4°C) in sterile 2% paraformaldehyde solution prepared in PBS. Fixed brains were cryoprotected in 15% sucrose overnight, followed by 30% sucrose overnight incubation (4°C). Cryoprotected brain hemispheres were horizontally sectioned through the VH at 30 μm and processed for FISH experiments. FISH was performed as described previously [31] with few modifications as follows. Slides were brought to room temperature, and all steps were performed at room temperature unless indicated otherwise. Warmed tissue sections were washed three times with 20 mM Glycine in 1X PBS 5 min each, followed by 3 washes in freshly prepared 25 mM $NaBH_4$ in 1X PBS, 5 min each. After a quick rinse with 0.1 M TEA, slices were washed in a 0.1 M TEA + 0.25% acetic anhydride solution for 10 min, followed by a 3 min wash in 2x SSC. Slices were then dehydrated in 70, 95, and 100% EtOH (3 min each), and immediately de-lipidized in chloroform for 5 min and rehydrated. Next, sections were washed 2 times in 2x SSC, followed by a quick wash in 0.3% triton X-100, before hybridization buffer was applied. *Nrg3* probes, *ErbB4* probes, and scrambled control probes were resuspended in TE buffer to a final concentration of 25 μM and added to hybridization buffer at 1:100 dilution. Hybridization was performed for 12-16 h at 37°C. Samples were then coverslipped the following day using Prolong Gold mounting medium with DAPI stain (Invitrogen) and analyzed by epifluorescent microscopy. Leica DMI6000 epifluorescent microscope with ORCA Flash ER CCD camera (Hamamatsu, Japan) was used for imaging unless otherwise specified. For quantification between samples, imaging parameters were matched for exposure, gain, offset, and post-processing. Scrambled probes were used as a control, and to assign image acquisition parameters that would minimize any nonspecific signal from the scrambled probe. *Nrg3* and *ErbB4* mRNA particle numbers were quantified using ImageJ and normalized to the number of nuclei. For each subregion (DG, CA3, CA1) of the VH, three images were taken, quantified, and averaged to represent an n of 1.

Whole-cell patch-clamp electrophysiology

24 h after minipump removal and immediately after behavioral testing, mice were sacrificed via live decapitation, brains were rapidly removed, and horizontal slices (300 μm-thick) containing the ventral hippocampus were cut using a vibratome (VT1200S; Leica Microsystems, Wetzlar, Germany) in an ice-cold cutting solution, containing the following (in mM): 93 NMDG, 2.5 KCl, 1.25 NaH_2PO_4, 30 $NaHCO_3$, 20 HEPES,

507   25 glucose, 5 Na-ascorbate, 2 thiourea, 3 Na-pyruvate, 10 $MgSO_4$, and 0.5 $CaCl_2$, adjusted to 300–310 mOsm,

508   pH 7.4 and continuously oxygenated with 95% O_2 and 5% CO_2. Slices were allowed to recover in the cutting

509   solution at 34–36°C for 30 min and were thereafter maintained in an oxygenated recording artificial cerebrospinal

510   fluid (aCSF) solution at room temperature. Recording aCSF contained the following (in mM): 130 NaCl, 3 KCl,

511   1.25 NaH_2PO_4, 26 $NaHCO_3$, 10 glucose, 1 $MgCl_2$, and 2 $CaCl_2$, pH 7.2–7.4, when saturated with 95% O_2 and

512   5% CO_2.

513   For electrophysiology recordings, recording pipettes were pulled from borosilicate glass capillaries (World

514   Precision Instruments, Sarasota, FL) to a resistance of 4–7 MΩ when filled with the intracellular solution. The

515   intracellular solution contained the following (in mM): 145 potassium gluconate, 2 $MgCl_2$, 2.5 KCl, 2.5 NaCl, 0.1

516   BAPTA, 10 HEPES, 2 Mg-ATP, and 0.5 GTP-Tris, pH 7.2–7.3, with KOH, osmolarity 280–290 mOsm. Brain

517   slices were transferred to the recording chamber continually perfused with carbogen-saturated recording aCSF

518   (1.5-2.0 ml/min) at 31–33°C. Pyramidal neurons in the CA1 region were viewed under an upright microscope

519   (Olympus BX51WI) with infrared differential interference contrast optics and a 40x water-immersion objective.

520   To evaluate spontaneous inhibitory postsynaptic currents (sIPSCs), the cells were voltage-clamped at 0 mV; to

521   evaluate spontaneous excitatory postsynaptic currents (sEPSCs), the cells were voltage-clamped at -70 mV. To

522   isolate miniature excitatory postsynaptic currents (mEPSCs) and miniature inhibitory postsynaptic currents

523   (mIPSCs), recording aCSF included 1 µM tetrodotoxin.

524   Currents were low pass filtered at 2 kHz and digitized at 20 kHz using a Digidata 1550B acquisition

525   system (Molecular Devices, San Jose, CA) coupled to the Multiclamp 700B amplifier (Molecular Devices) and

526   pClamp11 software (Molecular Devices). Access resistance (10–30 MΩ) was monitored during recordings by

527   injection of 10 mV hyperpolarizing pulses; data were discarded if access resistance changed >25% over the

528   course of data collection. All analyses were completed using Clampfit 11.1 (Molecular Devices).

529

530   *Calcium imaging*

531   Two-minute videos of Ca^{2+} fluorescence were acquired with an ORCA-Flash 4.0 (V2) digital camera

532   (Hamamatsu) via a 40x objective at 25 frames/second with a 512x512 pixel binning. Following imaging of

533   spontaneous Ca^{2+} transients, fluorescent signals in response to extracellular stimulation were recorded in each

534 field of view. Extracellular stimuli were delivered by 100 µs current pulses generated by a Master-9 stimulator

535 (A.M.P.I) via a bipolar tungsten electrode positioned just outside the field of view in the stratum radiatum. The

536 amplitude of the current pulses was controlled by a stimulus isolation unit (ISO-Flex, A.M.P.I.). Minimal

537 stimulation was defined as minimal current intensity to produce visible fluorescence in any of the imaged cells.

538 Network analysis of Ca^{2+} transients, was performed on the basis of undirected adjacency matrices thresholded

539 to preserve 25% of the strongest correlation coefficients as described in our previous publication [32].

540

541 *Data analyses*

542 Statistical analyses were performed with GraphPad Prism 6.0 software package (GraphPad Software,

543 San Diego, CA). Protein and mRNA analysis was performed using ordinary one-way or two-way ANOVA.

544 Behavioral measures, except where noted, were analyzed using two-way repeated- measures (RM) ANOVA as

545 test day or genotype as within-subject variables and drug treatment as a between-subject variable. Network

546 analyses of Ca^{2+} transients were done with one-way or two-way RM ANOVA, as indicated. ANOVA was followed

547 by Sidak's multiple comparison tests. For the electrophysiological studies, amplitudes of EPSCs and IPSCs were

548 computed from an average of 50–100 individual current traces. Mean EPSC and IPSC frequencies were

549 analyzed from 20 s long trace segments. EPSC and IPSC data were analyzed using 2-tailed Student's t-tests.

550 All data were expressed as mean ± SEM, and significance was set at $p < 0.05$.

551

555
556 **Author Contributions:** M.L.F. and J.R.T. contributed to the conception of the presented idea. M.L.F., T.A.,
557 P.S., J.L.T., P.I.O., and J.R.T. planned the experiments. M.L.F., E.R.P., B.O., T.A., P.S., J.L.T., and P.I.O.
558 carried out the experiments. All authors contributed to data analysis. M.L.F., E.R.P., P.I.O., and J.R.T. wrote
559 the manuscript.

560
561

References

1   American Society of Addiction Medicine I.   (2005).

2   De Biasi M, Salas R. Influence of neuronal nicotinic receptors over nicotine addiction and withdrawal. Exp Biol Med (Maywood). 2008;233(8):917-29.

3   Patten CA, Martin JE. Does nicotine withdrawal affect smoking cessation? Clinical and theoretical issues. Ann Behav Med. 1996;18(3):190-200.

4   Dani JA, Harris RA. Nicotine addiction and comorbidity with alcohol abuse and mental illness. Nat Neurosci. 2005;8(11):1465-70.

5   Hogle JM, Kaye JT, Curtin JJ. Nicotine withdrawal increases threat-induced anxiety but not fear: neuroadaptation in human addiction. Biol Psychiatry. 2010;68(8):719-25.

6   Picciotto MR, Brunzell DH, Caldarone BJ. Effect of nicotine and nicotinic receptors on anxiety and depression. Neuroreport. 2002;13(9):1097-106.

7   Piper ME, Cook JW, Schlam TR, Jorenby DE, Baker TB. Anxiety diagnoses in smokers seeking cessation treatment: relations with tobacco dependence, withdrawal, outcome and response to treatment. Addiction. 2011;106(2):418-27.

8   Pomerleau OF, Pomerleau CS, Mehringer AM, Snedecor SM, Ninowski R, Sen A. Nicotine dependence, depression, and gender: characterizing phenotypes based on withdrawal discomfort, response to smoking, and ability to abstain. Nicotine Tob Res. 2005;7(1):91-102.

9   Costall B, Kelly ME, Naylor RJ, Onaivi ES. The actions of nicotine and cocaine in a mouse model of anxiety. Pharmacol Biochem Behav. 1989;33(1):197-203.

10   Irvine EE, Cheeta S, File SE. Tolerance to nicotine's effects in the elevated plus-maze and increased anxiety during withdrawal. Pharmacol Biochem Behav. 2001;68(2):319-25.

11   Jackson KJ, Martin BR, Changeux JP, Damaj MI. Differential role of nicotinic acetylcholine receptor subunits in physical and affective nicotine withdrawal signs. J Pharmacol Exp Ther. 2008;325(1):302-12.

12   Jackson KJ, McIntosh JM, Brunzell DH, Sanjakdar SS, Damaj MI. The role of alpha6-containing nicotinic acetylcholine receptors in nicotine reward and withdrawal. J Pharmacol Exp Ther. 2009;331(2):547-54.

13   Fanselow MS, Dong HW. Are the dorsal and ventral hippocampus functionally distinct structures? Neuron. 2010;65(1):7-19.

14   Fisher ML, LeMalefant RM, Zhou L, Huang G, Turner JR. Distinct Roles of CREB Within the Ventral and Dorsal Hippocampus in Mediating Nicotine Withdrawal Phenotypes. Neuropsychopharmacology. 2017;42(8):1599-609.

15   Turner JR, Ray R, Lee B, Everett L, Xiang J, Jepson C, et al. Evidence from mouse and man for a role of neuregulin 3 in nicotine dependence. Mol Psychiatry. 2014;19(7):801-10.

16   Zhang D, Sliwkowski MX, Mark M, Frantz G, Akita R, Sun Y, et al. Neuregulin-3 (NRG3): a novel neural tissue-enriched protein that binds and activates ErbB4. Proc Natl Acad Sci U S A. 1997;94(18):9562-7.

17   Fujikawa A, Chow JP, Shimizu H, Fukada M, Suzuki R, Noda M. Tyrosine phosphorylation of ErbB4 is enhanced by PSD95 and repressed by protein tyrosine phosphatase receptor type Z. J Biochem. 2007;142(3):343-50.

18   Huang YZ, Won S, Ali DW, Wang Q, Tanowitz M, Du QS, et al. Regulation of neuregulin signaling by PSD-95 interacting with ErbB4 at CNS synapses. Neuron. 2000;26(2):443-55.

19   Murphy SP, Bielby-Clarke K. Neuregulin signaling in neurons depends on ErbB4 interaction with PSD-95. Brain Res. 2008;1207:32-5.

20   Bartolini G, Sánchez-Alcañiz JA, Osório C, Valiente M, García-Frigola C, Marín O. Neuregulin 3 Mediates Cortical Plate Invasion and Laminar Allocation of GABAergic Interneurons. Cell Rep. 2017;18(5):1157-70.

611 21 Mei L, Nave KA. Neuregulin-ERBB signaling in the nervous system and neuropsychiatric diseases.
612   Neuron. 2014;83(1):27-49.
613 22 Zhou L, Fisher ML, Cole RD, Gould TJ, Parikh V, Ortinski PI, et al. Neuregulin 3 Signaling Mediates
614   Nicotine-Dependent Synaptic Plasticity in the Orbitofrontal Cortex and Cognition.
615   Neuropsychopharmacology. 2018;43(6):1343-54.
616 23 Loukola A, Wedenoja J, Keskitalo-Vuokko K, Broms U, Korhonen T, Ripatti S, et al. Genome-wide
617   association study on detailed profiles of smoking behavior and nicotine dependence in a twin sample.
618   Mol Psychiatry. 2014;19(5):615-24.
619 24 Turner JR, Castellano LM, Blendy JA. Parallel anxiolytic-like effects and upregulation of neuronal
620   nicotinic acetylcholine receptors following chronic nicotine and varenicline. Nicotine Tob Res.
621   2011;13(1):41-6.
622 25 Turner JR, Castellano LM, Blendy JA. Nicotinic partial agonists varenicline and sazetidine-A have
623   differential effects on affective behavior. J Pharmacol Exp Ther. 2010;334(2):665-72.
624 26 Turner JR, Wilkinson DS, Poole RL, Gould TJ, Carlson GC, Blendy JA. Divergent functional effects of
625   sazetidine-a and varenicline during nicotine withdrawal. Neuropsychopharmacology. 2013;38(10):2035-
626   47.
627 27 Matta SG, Balfour DJ, Benowitz NL, Boyd RT, Buccafusco JJ, Caggiula AR, et al. Guidelines on
628   nicotine dose selection for in vivo research. Psychopharmacology (Berl). 2007;190(3):269-319.
629 28 Brynildsen JK, Najar J, Hsu LM, Vaupel DB, Lu H, Ross TJ, et al. A novel method to induce nicotine
630   dependence by intermittent drug delivery using osmotic minipumps. Pharmacol Biochem Behav.
631   2016;142:79-84.
632 29 Cleck JN, Ecke LE, Blendy JA. Endocrine and gene expression changes following forced swim stress
633   exposure during cocaine abstinence in mice. Psychopharmacology (Berl). 2008;201(1):15-28.
634 30 Livak KJ, Schmittgen TD. Analysis of relative gene expression data using real-time quantitative PCR
635   and the 2(-Delta Delta C(T)) Method. Methods. 2001;25(4):402-8.
636 31 Terenzio M, Koley S, Samra N, Rishal I, Zhao Q, Sahoo PK, et al. Locally translated mTOR controls
637   axonal local translation in nerve injury. Science. 2018;359(6382):1416-21.
638 32 O'Donovan B, Neugornet A, Neogi R, Xia M, Ortinski P. Cocaine experience induces functional
639   adaptations in astrocytes: Implications for synaptic plasticity in the nucleus accumbens shell. Addict
640   Biol. 2021;26(6):e13042.
641 33 Müller T, Braud S, Jüttner R, Voigt BC, Paulick K, Sheean ME, et al. Neuregulin 3 promotes excitatory
642   synapse formation on hippocampal interneurons. EMBO J. 2018;37(17).
643 34 Rio C, Buxbaum JD, Peschon JJ, Corfas G. Tumor necrosis factor-alpha-converting enzyme is required
644   for cleavage of erbB4/HER4. J Biol Chem. 2000;275(14):10379-87.
645 35 Merali Z, Levac C, Anisman H. Validation of a simple, ethologically relevant paradigm for assessing
646   anxiety in mice. Biol Psychiatry. 2003;54(5):552-65.
647 36 Cenquizca LA, Swanson LW. Spatial organization of direct hippocampal field CA1 axonal projections
648   to the rest of the cerebral cortex. Brain Res Rev. 2007;56(1):1-26.
649 37 Marr D. Simple memory: a theory for archicortex. Philos Trans R Soc Lond B Biol Sci.
650   1971;262(841):23-81.
651 38 Chen TW, Wardill TJ, Sun Y, Pulver SR, Renninger SL, Baohan A, et al. Ultrasensitive fluorescent
652   proteins for imaging neuronal activity. Nature. 2013;499(7458):295-300.
653 39 English DF, McKenzie S, Evans T, Kim K, Yoon E, Buzsáki G. Pyramidal Cell-Interneuron Circuit
654   Architecture and Dynamics in Hippocampal Networks. Neuron. 2017;96(2):505-20.e7.
655 40 Ortinski PI. Cocaine-induced changes in NMDA receptor signaling. Mol Neurobiol. 2014;50(2):494-
656   506.
657 41 Watkins SS, Koob GF, Markou A. Neural mechanisms underlying nicotine addiction: acute positive
658   reinforcement and withdrawal. Nicotine Tob Res. 2000;2(1):19-37.

| 659 | 42 | Rukstalis M, Jepson C, Patterson F, Lerman C. Increases in hyperactive-impulsive symptoms predict relapse among smokers in nicotine replacement therapy. J Subst Abuse Treat. 2005;28(4):297-304. |

659 42 Rukstalis M, Jepson C, Patterson F, Lerman C. Increases in hyperactive-impulsive symptoms predict
660 relapse among smokers in nicotine replacement therapy. J Subst Abuse Treat. 2005;28(4):297-304.
661 43 Patterson F, Jepson C, Loughead J, Perkins K, Strasser AA, Siegel S, et al. Working memory deficits
662 predict short-term smoking resumption following brief abstinence. Drug Alcohol Depend.
663 2010;106(1):61-4.
664 44 Malin DH, Goyarzu P. Rodent models of nicotine withdrawal syndrome. Handb Exp Pharmacol.
665 2009(192):401-34.
666 45 Malin DH, Lake JR, Newlin-Maultsby P, Roberts LK, Lanier JG, Carter VA, et al. Rodent model of
667 nicotine abstinence syndrome. Pharmacol Biochem Behav. 1992;43(3):779-84.
668 46 DiMatteo MR, Lepper HS, Croghan TW. Depression is a risk factor for noncompliance with medical
669 treatment: meta-analysis of the effects of anxiety and depression on patient adherence. Arch Intern Med.
670 2000;160(14):2101-7.
671 47 Hughes JR. Effects of abstinence from tobacco: valid symptoms and time course. Nicotine Tob Res.
672 2007;9(3):315-27.
673 48 Blendy JA, Maldonado R. Genetic analysis of drug addiction: the role of cAMP response element
674 binding protein. J Mol Med (Berl). 1998;76(2):104-10.
675 49 Carlezon WA, Duman RS, Nestler EJ. The many faces of CREB. Trends Neurosci. 2005;28(8):436-45.
676 50 Nestler EJ. Is there a common molecular pathway for addiction? Nat Neurosci. 2005;8(11):1445-9.
677 51 Stoker AK, Semenova S, Markou A. Affective and somatic aspects of spontaneous and precipitated
678 nicotine withdrawal in C57BL/6J and BALB/cByJ mice. Neuropharmacology. 2008;54(8):1223-32.
679 52 McLaughlin I, Dani JA, De Biasi M. Nicotine withdrawal. Curr Top Behav Neurosci. 2015;24:99-123.
680 53 McClernon FJ, Kozink RV, Rose JE. Individual differences in nicotine dependence, withdrawal
681 symptoms, and sex predict transient fMRI-BOLD responses to smoking cues.
682 Neuropsychopharmacology. 2008;33(9):2148-57.
683 54 Froeliger B, Kozink RV, Rose JE, Behm FM, Salley AN, McClernon FJ. Hippocampal and striatal gray
684 matter volume are associated with a smoking cessation treatment outcome: results of an exploratory
685 voxel-based morphometric analysis. Psychopharmacology (Berl). 2010;210(4):577-83.
686 55 Vullhorst D, Ahmad T, Karavanova I, Keating C, Buonanno A. Structural Similarities between
687 Neuregulin 1-3 Isoforms Determine Their Subcellular Distribution and Signaling Mode in Central
688 Neurons. J Neurosci. 2017;37(21):5232-49.
689 56 Vullhorst D, Neddens J, Karavanova I, Tricoire L, Petralia RS, McBain CJ, et al. Selective expression of
690 ErbB4 in interneurons, but not pyramidal cells, of the rodent hippocampus. J Neurosci.
691 2009;29(39):12255-64.
692 57 Kao WT, Wang Y, Kleinman JE, Lipska BK, Hyde TM, Weinberger DR, et al. Common genetic
693 variation in Neuregulin 3 (NRG3) influences risk for schizophrenia and impacts NRG3 expression in
694 human brain. Proc Natl Acad Sci U S A. 2010;107(35):15619-24.
695 58 Cheng QC, Tikhomirov O, Zhou W, Carpenter G. Ectodomain cleavage of ErbB-4: characterization of
696 the cleavage site and m80 fragment. J Biol Chem. 2003;278(40):38421-7.
697 59 Ni CY, Murphy MP, Golde TE, Carpenter G. gamma -Secretase cleavage and nuclear localization of
698 ErbB-4 receptor tyrosine kinase. Science. 2001;294(5549):2179-81.
699 60 Sardi SP, Murtie J, Koirala S, Patten BA, Corfas G. Presenilin-dependent ErbB4 nuclear signaling
700 regulates the timing of astrogenesis in the developing brain. Cell. 2006;127(1):185-97.
701 61 Carpenter G. ErbB-4: mechanism of action and biology. Exp Cell Res. 2003;284(1):66-77.
702 62 Bailey KR, Crawley JN. Anxiety-Related Behaviors in Mice. In: Buccafusco JJ, editor Methods of
703 Behavior Analysis in Neuroscience. Boca Raton (FL): CRC Press/Taylor & Francis; 2009.
704 63 Yohn NL, Turner JR, Blendy JA. Activation of α4β2*/α6β2* nicotinic receptors alleviates anxiety
705 during nicotine withdrawal without upregulating nicotinic receptors. J Pharmacol Exp Ther.
706 2014;349(2):348-54.

707 64   Santarelli L, Gobbi G, Blier P, Hen R. Behavioral and physiologic effects of genetic or pharmacologic
708   inactivation of the substance P receptor (NK1). J Clin Psychiatry. 2002;63:11-17.
709 65   Gross C, Zhuang X, Stark K, Ramboz S, Oosting R, Kirby L, et al. Serotonin1A receptor acts during
710   development to establish normal anxiety-like behaviour in the adult. Nature. 2002;416(6879):396-400.
711 66   Cloninger CR. A unified biosocial theory of personality and its role in the development of anxiety states.
712   Psychiatr Dev. 1986;4(3):167-226.
713 67   Piazza PV, Deminiere JM, Maccari S, Mormede P, Le Moal M, Simon H. Individual reactivity to
714   novelty predicts probability of amphetamine self-administration. Behav Pharmacol. 1990;1(4):339-45.
715 68   Li WW, Yu H, Miller DJ, Yang F, Rouen C. Novelty Seeking and Mental Health in Chinese University
716   Students Before, During, and After the COVID-19 Pandemic Lockdown: A Longitudinal Study. Front
717   Psychol. 2020;11:600739.
718 69   Stedenfeld KA, Clinton SM, Kerman IA, Akil H, Watson SJ, Sved AF. Novelty-seeking behavior
719   predicts vulnerability in a rodent model of depression. Physiol Behav. 2011;103(2):210-6.
720 70   Paterson C, Law AJ. Transient overexposure of neuregulin 3 during early postnatal development
721   impacts selective behaviors in adulthood. PLoS One. 2014;9(8):e104172.
722 71   Del Pino I, García-Frigola C, Dehorter N, Brotons-Mas JR, Alvarez-Salvado E, Martínez de Lagrán M,
723   et al. Erbb4 deletion from fast-spiking interneurons causes schizophrenia-like phenotypes. Neuron.
724   2013;79(6):1152-68.
725 72   Geng HY, Zhang J, Yang JM, Li Y, Wang N, Ye M, et al. Deletion from Medium Spiny Neurons of the
726   Nucleus Accumbens Core Induces Schizophrenia-Like Behaviors via Elevated GABA. J Neurosci.
727   2017;37(31):7450-64.
728 73   Cao SX, Zhang Y, Hu XY, Hong B, Sun P, He HY, et al. ErbB4 deletion in noradrenergic neurons in the
729   locus coeruleus induces mania-like behavior via elevated catecholamines. Elife. 2018;7.
730 74   Zhang SR, Wu JL, Chen H, Luo R, Chen WJ, Tang LJ, et al. ErbB4 knockdown in serotonergic neurons
731   in the dorsal raphe induces anxiety-like behaviors. Neuropsychopharmacology. 2020;45(10):1698-706.
732 75   Ahrens S, Wu MV, Furlan A, Hwang GR, Paik R, Li H, et al. A Central Extended Amygdala Circuit
733   That Modulates Anxiety. J Neurosci. 2018;38(24):5567-83.
734 76   Bi LL, Sun XD, Zhang J, Lu YS, Chen YH, Wang J, et al. Amygdala NRG1-ErbB4 is critical for the
735   modulation of anxiety-like behaviors. Neuropsychopharmacology. 2015;40(4):974-86.
736 77   Geng F, Zhang J, Wu JL, Zou WJ, Liang ZP, Bi LL, et al. Neuregulin 1-ErbB4 signaling in the bed
737   nucleus of the stria terminalis regulates anxiety-like behavior. Neuroscience. 2016;329:182-92.
738 78   Kjaerby C, Athilingam J, Robinson SE, Iafrati J, Sohal VS. Serotonin 1B Receptors Regulate Prefrontal
739   Function by Gating Callosal and Hippocampal Inputs. Cell Rep. 2016;17(11):2882-90.
740 79   Padilla-Coreano N, Bolkan SS, Pierce GM, Blackman DR, Hardin WD, Garcia-Garcia AL, et al. Direct
741   Ventral Hippocampal-Prefrontal Input Is Required for Anxiety-Related Neural Activity and Behavior.
742   Neuron. 2016;89(4):857-66.
743 80   Parfitt GM, Nguyen R, Bang JY, Aqrabawi AJ, Tran MM, Seo DK, et al. Bidirectional Control of
744   Anxiety-Related Behaviors in Mice: Role of Inputs Arising from the Ventral Hippocampus to the
745   Lateral Septum and Medial Prefrontal Cortex. Neuropsychopharmacology. 2017;42(8):1715-28.
746 81   Adhikari A, Topiwala MA, Gordon JA. Synchronized activity between the ventral hippocampus and the
747   medial prefrontal cortex during anxiety. Neuron. 2010;65(2):257-69.
748 82   Schoenfeld TJ, Kloth AD, Hsueh B, Runkle MB, Kane GA, Wang SS, et al. Gap junctions in the ventral
749   hippocampal-medial prefrontal pathway are involved in anxiety regulation. J Neurosci.
750   2014;34(47):15679-88.
751 83   Jimenez JC, Su K, Goldberg AR, Luna VM, Biane JS, Ordek G, et al. Anxiety Cells in a Hippocampal-
752   Hypothalamic Circuit. Neuron. 2018;97(3):670-83.e6.
753 84   Felix-Ortiz AC, Beyeler A, Seo C, Leppla CA, Wildes CP, Tye KM. BLA to vHPC inputs modulate
754   anxiety-related behaviors. Neuron. 2013;79(4):658-64.

755   85   Felix-Ortiz AC, Tye KM. Amygdala inputs to the ventral hippocampus bidirectionally modulate social
756   behavior. J Neurosci. 2014;34(2):586-95.
757   86   Klausberger T, Somogyi P. Neuronal diversity and temporal dynamics: the unity of hippocampal circuit
758   operations. Science. 2008;321(5885):53-7.
759   87   Neddens J, Buonanno A. Selective populations of hippocampal interneurons express ErbB4 and their
760   number and distribution is altered in ErbB4 knockout mice. Hippocampus. 2010;20(6):724-44.
761   88   Mitchell RM, Janssen MJ, Karavanova I, Vullhorst D, Furth K, Makusky A, et al. ErbB4 reduces
762   synaptic GABAA currents independent of its receptor tyrosine kinase activity. Proc Natl Acad Sci U S
763   A. 2013;110(48):19603-8.
764   89   Bean JC, Lin TW, Sathyamurthy A, Liu F, Yin DM, Xiong WC, et al. Genetic labeling reveals novel
765   cellular targets of schizophrenia susceptibility gene: distribution of GABA and non-GABA ErbB4-
766   positive cells in adult mouse brain. J Neurosci. 2014;34(40):13549-66.
767   90   Exposito-Alonso D, Osorio C, Bernard C, Pascual-Garcia S, Del Pino I, Marin O, et al. Subcellular
768   sorting of neuregulins controls the assembly of excitatory-inhibitory cortical circuits. Elife. 2020;9.
769   91   Chen YJ, Zhang M, Yin DM, Wen L, Ting A, Wang P, et al. ErbB4 in parvalbumin-positive
770   interneurons is critical for neuregulin 1 regulation of long-term potentiation. Proc Natl Acad Sci U S A.
771   2010;107(50):21818-23.
772   92   Fujii S, Ji Z, Sumikawa K. Inactivation of alpha7 ACh receptors and activation of non-alpha7 ACh
773   receptors both contribute to long term potentiation induction in the hippocampal CA1 region. Neurosci
774   Lett. 2000;286(2):134-8.
775   93   Asede D, Okoh J, Ali S, Doddapaneni D, Bolton MM. Deletion of ErbB4 Disrupts Synaptic
776   Transmission and Long-Term Potentiation of Thalamic Input to Amygdalar Medial Paracapsular
777   Intercalated Cells. Front Synaptic Neurosci. 2021;13:697110.
778   94   Woo RS, Li XM, Tao Y, Carpenter-Hyland E, Huang YZ, Weber J, et al. Neuregulin-1 enhances
779   depolarization-induced GABA release. Neuron. 2007;54(4):599-610.
780   95   Pitcher GM, Beggs S, Woo RS, Mei L, Salter MW. ErbB4 is a suppressor of long-term potentiation in
781   the adult hippocampus. Neuroreport. 2008;19(2):139-43.
782   96   Wen L, Lu YS, Zhu XH, Li XM, Woo RS, Chen YJ, et al. Neuregulin 1 regulates pyramidal neuron
783   activity via ErbB4 in parvalbumin-positive interneurons. Proc Natl Acad Sci U S A. 2010;107(3):1211-
784   6.
785

Figures and Figure Legends
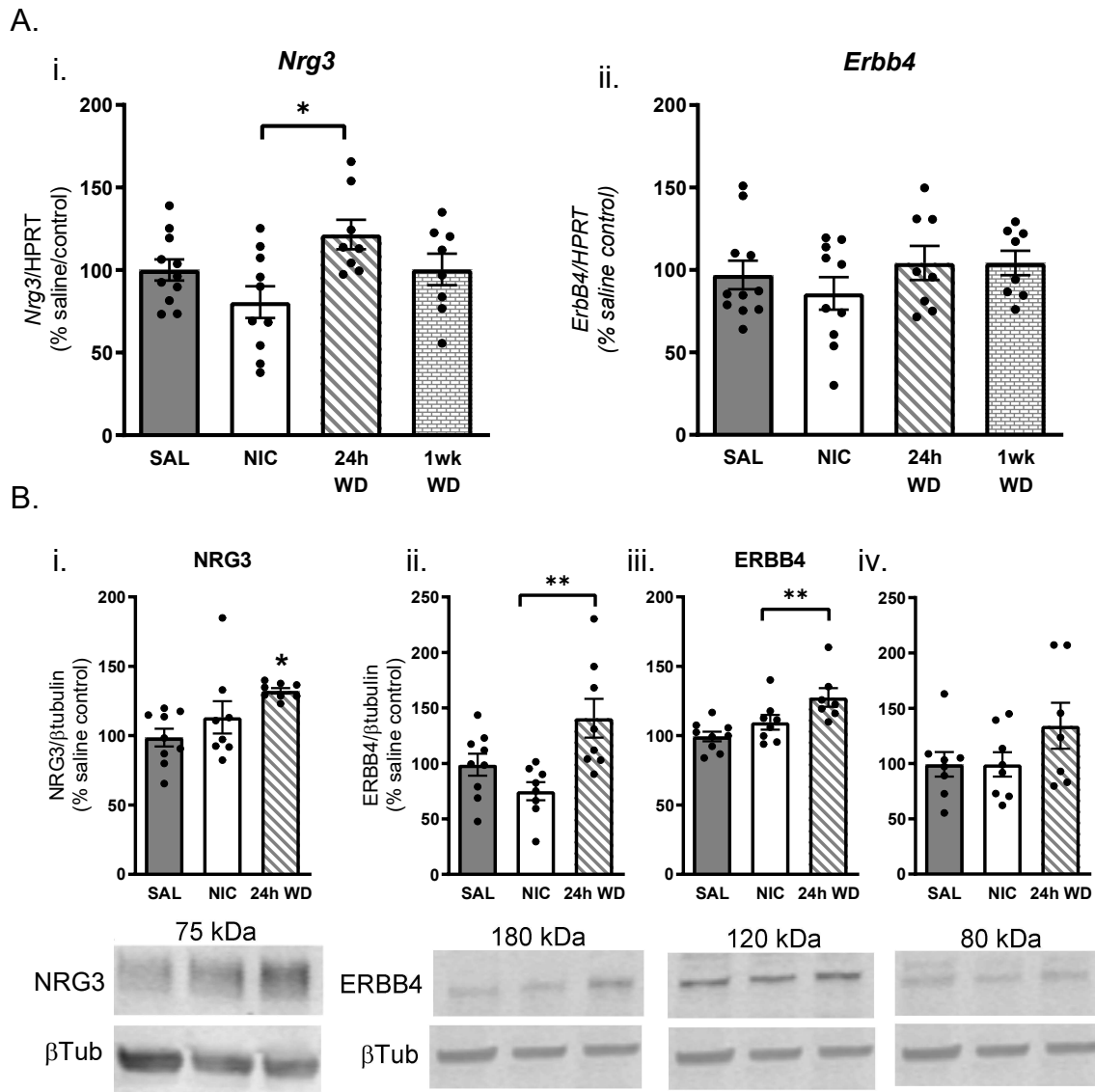
Figure 1. 24hWD increases VH expression of NRG3 and ERBB4.

(A) mRNA quantification of (i) *Nrg3* and (ii) *ErbB4*. (B) densitometry analysis of (i) synaptosomal NRG3 (75kDa band) protein, and synaptosomal ERBB4 protein at (ii) 180kDa, (iii) 120kDa, and (iv) 80kDa bands in treated ventral hippocampal murine tissue. The same Beta-tubulin control for ERBB4 analysis is shown in Bii, iii, and iv, as the analysis was conducted on a single gel. N=8-10 per group (*p<0.05, **p<0.01).

27
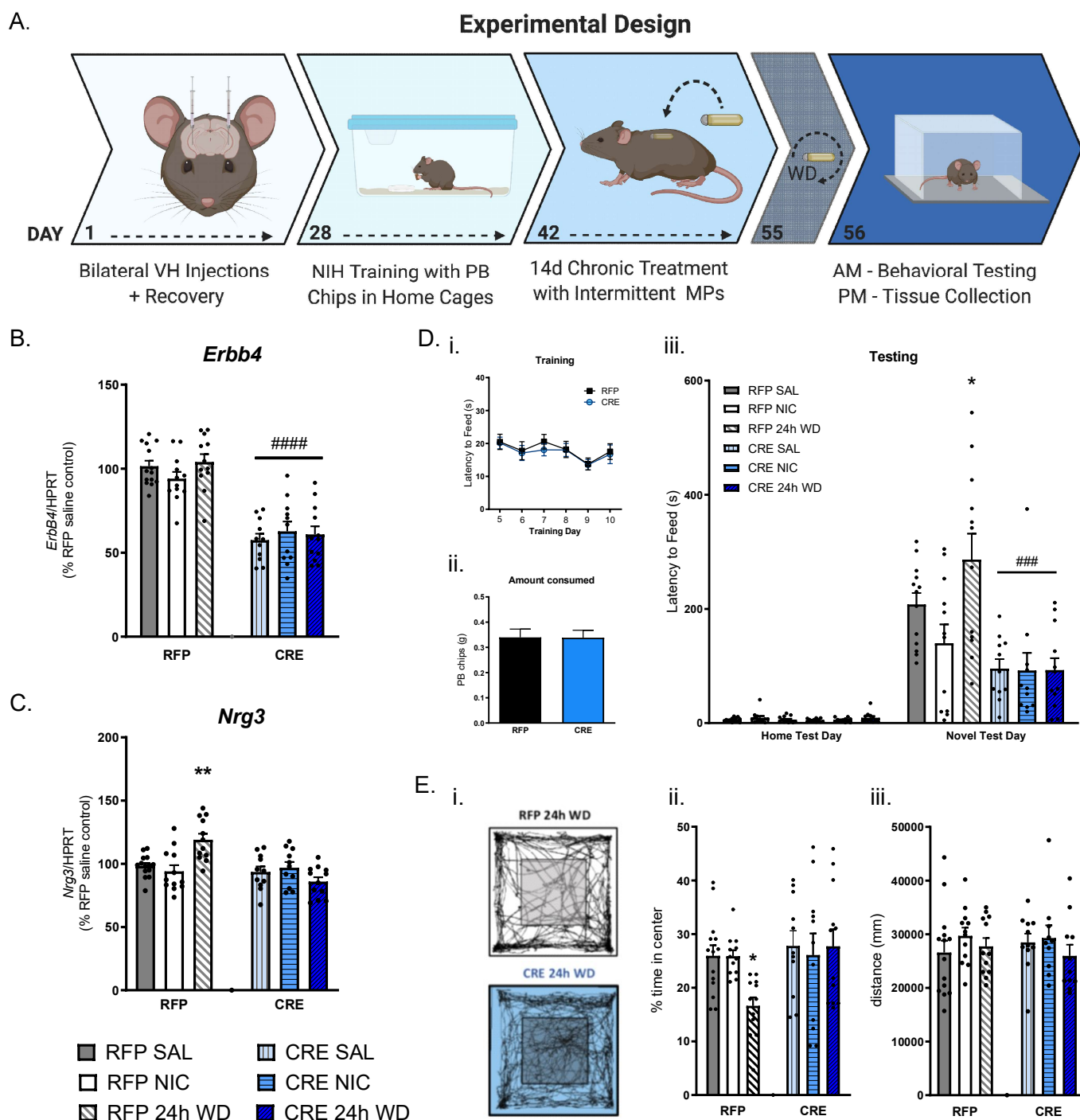
Figure 2. Gene expression analysis of VH *ErbB4* knock-down and consequent attenuation of nicotine WD-induced anxiety-like behavior.

(A) Experimental Design. (B) Quantification of *ErbB4* mRNA in CRE-injected mice compared to RFP-injected controls. (C) Quantification of *Nrg3* mRNA in CRE-injected mice compared to RFP-injected controls. n=11-14 per group. (*p<0.05, treatment effect; ##p<0.01, ####p<0.0001, viral effect). (D) Novelty-induced hypophagia

28

801   (NIH) test. (i) Latency to feed in RFP and CRE-injected animals during NIH training prior to treatment. (ii) Amount

802   of peanut butter chips (PB) consumed in RFP and CRE-injected animals on NIH training day 10. (iii) Latency to

803   feed in treated, RFP and CRE-injected animals in home cage (Home Test Day) and novel environment (Novel

804   Test Day). (E) Open Field exploratory test. (i) Representative activity traces in RFP and CRE-injected mice

805   undergoing 24hWD. (ii) Measurement of percent time spent in the center arena of treated RFP- and CRE-injected

806   mice. (iii) Locomotor activity of RFP- and CRE-injected mice in arena. N=11-14 per group. (*p<0.05, treatment

807   effect; ###p<0.001, viral effect).

808

809
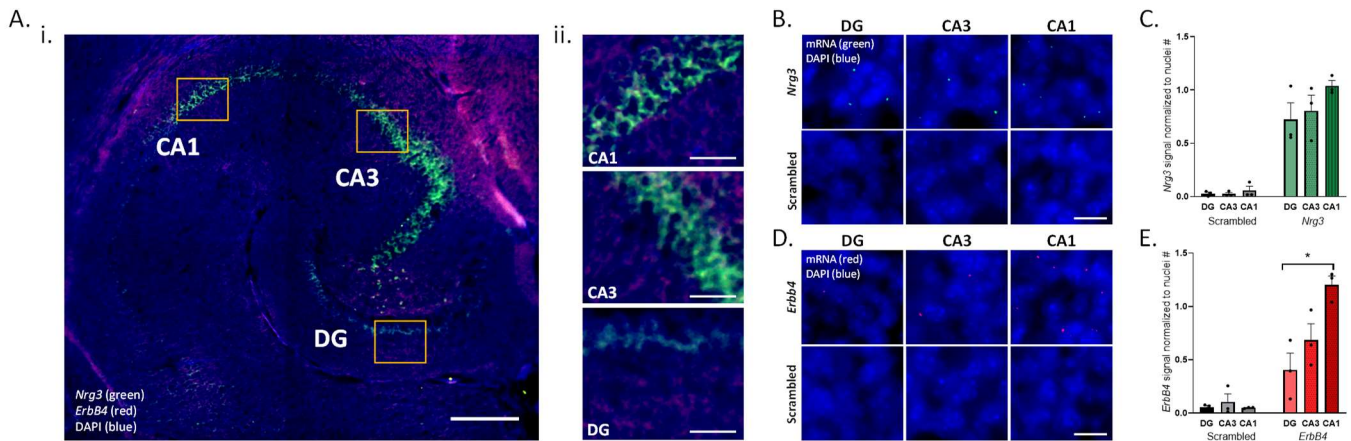
Figure 3. *Nrg3* and *ErbB4* mRNA expression predominates in the CA1 region of the VH.

Representative horizontal 30 µm VH sections from untreated mice, incubated with either Stellaris probe against

Nrg3 or *ErbB4* mRNAs or scrambled probes. Background subtractions are based on scrambled control images.

(A) Representative 10x image of *Nrg3* (green) and *ErbB4* (red) mRNA labeled with Stellaris RNA FISH probes,

and DAPI stain (blue) in (i) the VH (Scale bar 300 µm), and (ii) subareas DG, CA3, and CA1 (Scale bar 50 µm).

(B) Representative 63x oil immersion images *Nrg3* mRNA puncta (green) and DAPI (blue) in the DG, CA3, CA1

of VH (Scale bar 20 µm). (C) Quantification of *Nrg3* mRNA normalized to nuclei number. (D) Representative 63x

oil immersion images of *ErbB4* mRNA puncta (green) and DAPI (blue) in the DG, CA3, and CA1 of VH. (E)

Quantification of *ErbB4* mRNA normalized to nuclei number (scale bar 20 µm). N=3 per group. (*p<0.05).

819
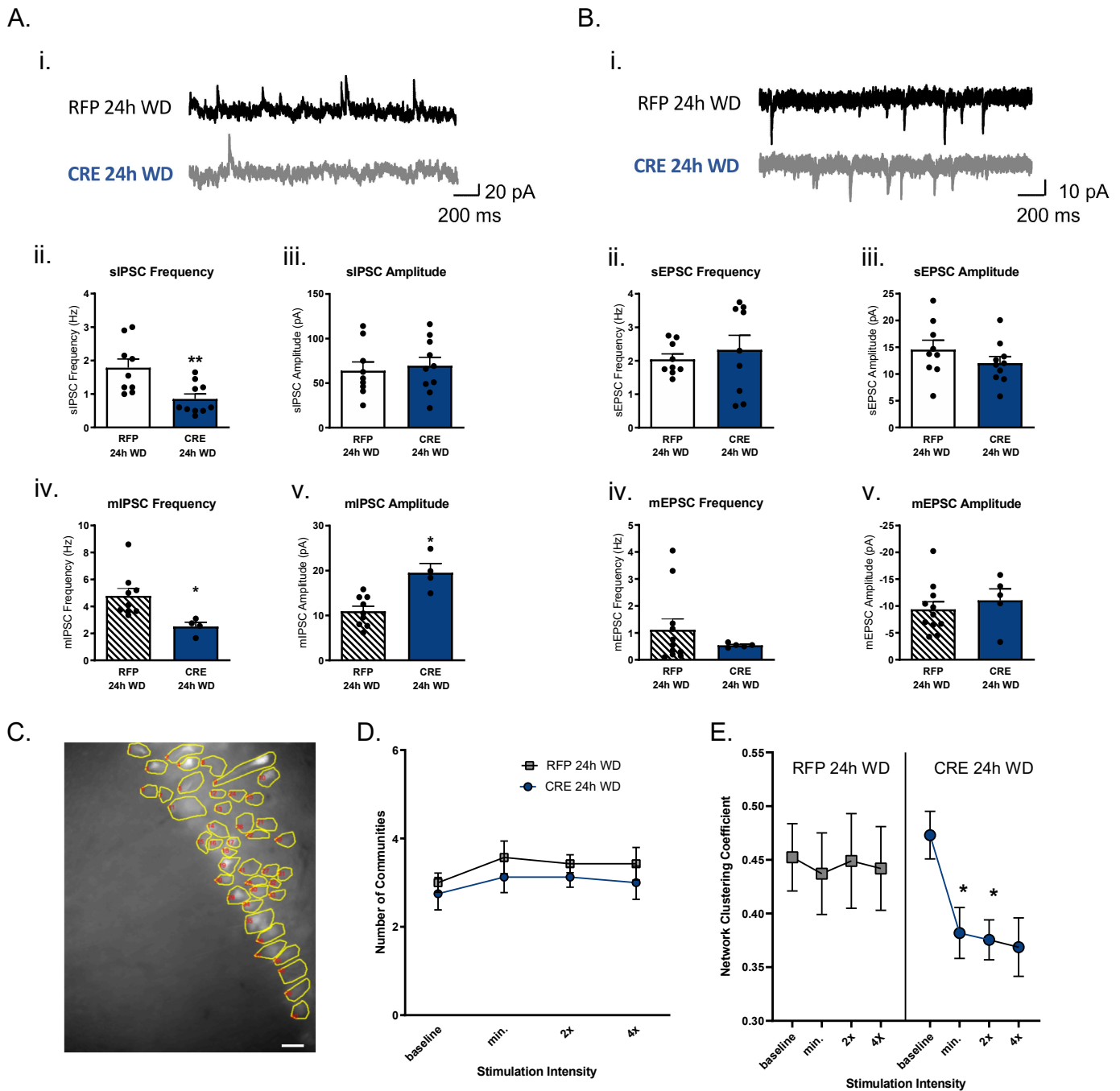
Figure 4. Ventral hippocampal *ErbB4* knock-down reduces spontaneous IPSC frequency and Ca²⁺-dependent network clustering during 24hWD.

(A) Whole cell patch clamp recordings of spontaneous and miniature inhibitory post-synaptic currents (sIPSCs/mIPSCs). (i) Representative sIPSC traces. Quantification of sIPSC (ii) frequency and (iii) amplitude and mIPSC (iv) frequency and (v) amplitude in RFP- and CRE-injected mice undergoing 24hWD. (B) Whole cell patch clamp recordings of spontaneous and mini excitatory post-synaptic currents (sEPSCs/mEPSCs). (i)

827   Representative sEPSC traces. Quantification of sEPSC (ii) frequency and (iii) amplitude and mEPSC (iv)

828   frequency and (v) amplitude in RFP- and CRE-injected mice undergoing 24hWD. N=4 animals (2-3 cells per

829   animal) (**p<0.01). (C) Representative 40x image of fluorescently GCaMP6f-labelled ventral CA1 pyramidal cells

830   outlines as numbered ROIs (scale bar 30 microns). (D) Quantification of ventral CA1 pyramidal cell

831   communicatees across increasing stimulation intensities in RFP- and CRE-injected mice undergoing 24hWD.

832   (E) Quantification of network clustering coefficient across increasing stimulation intensities in RFP- and CRE-

833   injected mice undergoing 24hWD. N=4 mice (2-3 sections per animal (*p<0.05).

834

835 **Supplemental Materials**

836
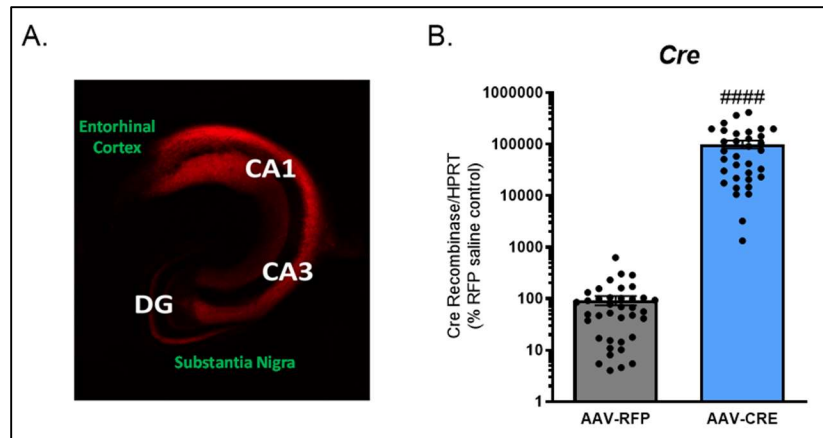
837

838 **Figure S1. Viral expression analysis of VH CRE recombinase.**

839 (A) Representative con-focal image of RFP in VH (white) and non-expressing (green) regions. (B)

840 Quantification via RTqPCR analyses of CRE recombinase mRNA in RFP- and CRE-injected mice

841 (####p<0.0001).

842
843

33

844 **Table S1.** RTqPCR Primers

Gene name (CT)	Forward strand (5'3')	Reverse strand (5'3')
HPRT (21)	CAAAGCCTAAGATGAGCGCAAG	TTACTAGGCAGATGGCCACAGG
NRG3 (26)	CAGCTGTGGTGTGTTGAAAGA	GGGGTTTGTCTCTCTTGAAGG
ErbB4 (25)	ACAACCAGCACCATACCAGAG	TGTCATGCATTGGAGTCATGT

845 Abbreviations: CT, cycle threshold; HPRT, hypoxanthine phosphoribosyltransferase; NRG3,
846 Neuregulin 3; qPCR, quantitative PCR
847
848